Chapter 5

Evolution of and Dynamics Within Streams

Stellar streams are known to contain intrinsic substructure that has the potential to be mistaken for external kinematic perturbations (e.g., from passing spiral arms, giant molecular clouds, or dark matter subhalos). The morphological appearance of these substructures and their dynamical formation mechanisms vary across the spectrum of Galactic satellites, but in this chapter we will limit ourselves to considering satellites forming streams in the relaxation limited regime—dense globular clusters—where the substructure is coldest and most coherent.

We will begin by building the analytical framework used to describe the "epicyclic" motion of stars in the streams of clusters on circular orbits, before discussing the validity of its extension to eccentric orbits.

5.1 Some relevant background

For the most part the details of this section is are not important, but are meant to demonstrate the problem that the epicycle approximation aims to simplify.

Orbits in an axisymmetric potential can be described in the "meridional plane" (that is, the (R, z) plane in cylindrical coordinates). For potential $\Phi(R, z)$, the Hamiltonian is written (Bovy 2026; sec 9.1)

$$H(R, \phi, z, p_R, p_\phi, p_z) = \frac{1}{2m}(p_R^2 + p_z^2) + m\Phi(R, z) + \frac{p_\phi^2}{2mR^2}. \tag{5.1}$$

Since the final term can be written in terms of L_z, a conserved integral of motion in an axisymmetric potential about the z-axis, we use it to define the "effective potential"

$$\Phi_{\text{eff}}(R, z; L_z) = \Phi(R, z) + \frac{p_\phi^2}{2mR^2} = \Phi(R, z) + \frac{L_z^2}{2R^2} \tag{5.2}$$

and the "effective Hamiltonian"

$$H_{\text{eff}}(R, z; L_z) = \frac{1}{2m}(p_R^2 + p_z^2) + m\Phi_{\text{eff}}(R, z) \tag{5.3}$$

These are helpful because we have completely flattened our problem into four phase space dimensions (position and momentum along R and z) down from six.

We can now write down the equations of motion using Hamilton's equations (see Bovy 2026, §3.4.1) in terms of the effective potential:

$$\begin{aligned} \ddot{R} &= -\frac{\partial \Phi_{\text{eff}}}{\partial R} = -\frac{\partial \Phi}{\partial R} + \frac{L_z^2}{R^3} \\ \ddot{z} &= -\frac{\partial \Phi_{\text{eff}}}{\partial z} = -\frac{\partial \Phi}{\partial z}. \end{aligned} \tag{5.4}$$

Below are few points other points from §9.1 of Bovy (2026) that will be useful momentarily: First, the effective potential grows large as $R \to 0$ (while for typical galactic potentials $\Phi(R, z)$ decreases at small R, their R-dependence is less steep than the $1/R^2$ dependence of the angular momentum term). See Figure 5.1. Orbits cannot reach $R = 0$.

Second, the minimum of the effective potential is in the plane of the disk at some $R_{\text{min,eff}}$, which for a given L_z can be reached by a circular orbit in the disk with velocity $v_c(R_{\text{min,eff}})$ such that $L_z = R_{\text{min,eff}} v_c$. The radius of a circular orbit with specific angular momentum L_z is called the **guiding center radius** and written R_g. Again, see Figure 5.1.

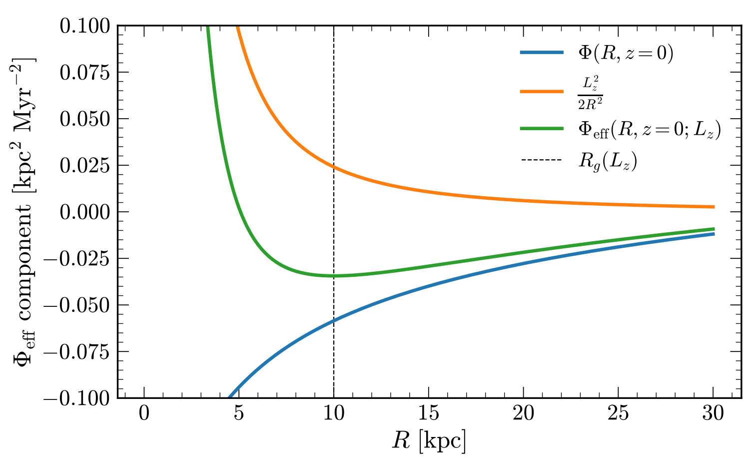

Figure 5.1: For $z = 0$, the value of Φ (using `MWPotential2014` as generated by `gala`), $L_z^2/(2R^2)$, and the combined Φ_{eff}. L_z was chosen so that the guiding center radius is 10 kpc.

Finally, the equations of motion dictate oscillations about the minimum of Φ_{eff} located at $(R_g, 0)$. Importantly, though, **because typical galactic potentials $\Phi(R, z)$ and Φ_{eff}** (including `MWPotential2014`) **cannot be separated into R- and z-dependent components, the oscillations in R and z are coupled.**

5.2 Nearly circular orbits and the epicycle approximation

Consider a nearly circular orbit (with R always very close to R_g and z always near zero) with angular momentum L_z. We can approximate the effective potential by Taylor expanding it around $(R_g, 0)$:

$$\Phi_{\text{eff}}(R, z; L_z) \approx \Phi_{\text{eff}}(R_g, 0; L_z) + \frac{1}{2}\left(\frac{\partial^2\Phi_{\text{eff}}}{\partial R^2}\right)\bigg|_{(R_g,0)}(R - R_g)^2 + \frac{1}{2}\left(\frac{\partial^2\Phi_{\text{eff}}}{\partial z^2}\right)\bigg|_{(R_g,0)} z^2, \quad (5.5)$$

where the first partial terms vanish since $(R_g, 0)$ is a minimum. We see that now the effective potential is split into components that depend on R and z separately. Using Hamilton's equations in cylindrical coordinates again, we find the new equations of motion (noting that $\ddot{R}_g = 0$):

$$\begin{aligned}\ddot{R} = \ddot{R} - \ddot{R}_g &= -\left(\frac{\partial^2\Phi_{\text{eff}}}{\partial R^2}\right)\bigg|_{(R_g,0)}(R - R_g) \\ \ddot{z} &= -\left(\frac{\partial^2\Phi_{\text{eff}}}{\partial z^2}\right)\bigg|_{(R_g,0)} z\end{aligned} \quad (5.6)$$

We have explicitly decoupled the oscillations about the minimum of Φ_{eff} into R and z components. The above are just the equations of motion of two harmonic oscillators with frequencies

$$\begin{aligned}\kappa^2(R_g) &= \left(\frac{\partial^2\Phi_{\text{eff}}}{\partial R^2}\right)\bigg|_{(R_g,0)} \\ \nu^2(R_g) &= \left(\frac{\partial^2\Phi_{\text{eff}}}{\partial z^2}\right)\bigg|_{(R_g,0)}\end{aligned} \quad (5.7)$$

κ is called the "epicycle" or the "radial" frequency, and ν is the "vertical frequency." A third important frequency is the azimuthal frequency $\Omega(R_g)$ of the circular orbit at the guiding center radius:

$$\Omega(R_g) = \frac{v_c(R_g)}{R_g} = \frac{L_z}{R_g^2}. \quad (5.8)$$

It is straightforward to now solve the harmonic oscillator equations of motion to find the motion in z and R_g.

$$\begin{aligned}z(t) &= A_z \cos(\nu t + \zeta) \\ R(t) - R_g &= A_R \cos(\kappa t + \alpha),\end{aligned} \quad (5.9)$$

where A_z, ζ, A_R, α are determined by the initial conditions. The dependence of the motion on the potential is captured through κ, ν from Equations 5.7.

To find the full orbit, we also need the azimuthal motion, which we can find by conserving angular momentum: $R^2\dot{\phi} = L_z$:

$$\dot{\phi} = \frac{L_z}{(R_g + [R(t) - R_g])^2} \approx \frac{L_z}{R_g^2}\left(1 - 2\frac{R(t) - R_g}{R_g}\right), \tag{5.10}$$

where in the last step we have used the binomial approximation, assuming that $(R - R_g)/R_g \ll 1$. Substituting our expression for $R(t) - R_g$, using $\Omega = L_z/R_g^2$, and integrating, we find

$$\phi(t) = \phi_0 + \Omega t - 2\frac{\Omega}{\kappa}\frac{A_R}{R_g}\sin(\kappa t - \alpha) \tag{5.11}$$

for initial azimuthal coordinate ϕ_0. The motion of the guiding center itself is given by $(R, \phi)[t] = (R_g, \Omega t + \phi_0)$. When we subtract this away from the $\phi(t)$ component of the orbit, we find motion relative to the guiding center:

$$R(t) - R_g = A_R\cos(\kappa t + \alpha); \quad R_g(\phi(t) - \Omega t - \phi_0) = -2\frac{\Omega}{\kappa}\frac{A_R}{R_g}\sin(\kappa t + \alpha). \tag{5.12}$$

Here I have copied notation from Bovy (2026) (eq. 9.23) even though I find it confusing. If we ignore the fact that $\phi(t)$ is an angle and instead imagine cartesian-like coordinate axes in the plane of the disk defining the directions of R and ϕ, we see that Equations 5.12 parameterize motion in an ellipse centered on the guiding center and with axis ratio $\gamma = \frac{2\Omega}{\kappa}$. κ gives the frequency at which a star travels around its epicycle ellipse.

See B&T §3.5.3b or Beane et al. (2019) for a description of the epicycle approximation in action space.

How does this manifest as substructure in a stellar stream? Imagine a cluster on a circular orbit in the disk (i.e., not executing any epicyclic motion). As stars escape the cluster, they are inserted onto nearly but no longer circular orbits, with guiding center radii inside (outside) that of the progenitor in the leading (trailing) tails. The escaped stars begin to execute epicyclic motion about their new guiding centers. Figure 5.2 shows a schematic of how this occurs. A cluster is on a circular orbit of radius R_C with angular velocity Ω_C. The guiding centers of the epicycles (or "epicenters") of escaping stars are located at $R_0^{(\prime)} = R_C \pm \Delta R$, and have angular velocities $\Omega_0^{(\prime)} = \Omega_C \pm \Delta\Omega$. The inner epicenters race ahead of the cluster on its orbit while the outer epicenters lag behind. The combined epicyclic motion of the escaping stars and the differential rotation of the epicenters themselves gives rise to cuspy features where the stars come to rest at the end of one epicycle before beginning the next one. Because the tangential velocity along the stream is smallest at the cusps (i.e.,

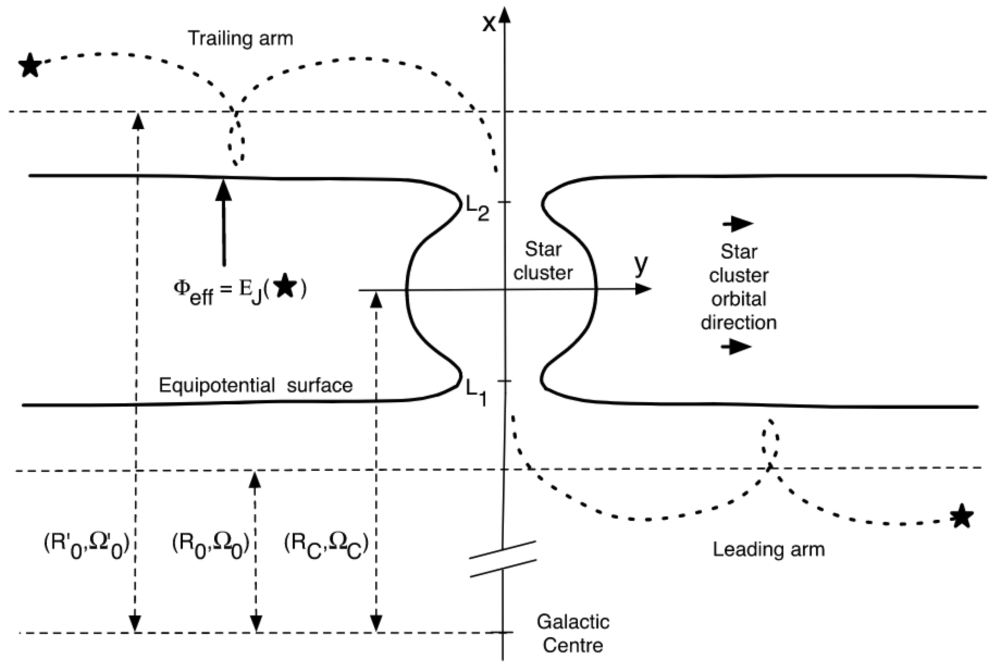

Figure 5.2: From Just et al. (2009), a schematic of the epicyclic motion of stars escaping an orbiting cluster.

stars spend more time at the cusps), the epicyclic motion creates overdensities of stars at the cusps (this is how we would detect the presence of epicycles if we viewed the stream in projection to the y-z plane in these figures). Figure 5.3 colors stream stars by local density, so we can see this effect clearly.

Although the epicyclic frequency in *time* κ is determined by the host potential, the offset of the epicenters from the cluster's orbit and the radial amplitudes of the oscillations (A_R in Equation 5.12) depend on the angular momentum offsets of escaping stars compared to the cluster and their energies in excess of the cluster's escape energy, respectively. Characterizing typical distributions of escape conditions that determine these (e.g., the radii at which stars become unbound and begin epicyclic motion, the typical velocity offsets in the radial and tangential directions, and the dispersion in each) is an area of ongoing research (e.g., see Fardal et al. 2015; Weatherford et al. 2023). Stars released at positions radially further from the cluster and with zero velocity offset will oscillate about epicenters with larger offsets in angular speed compared to the progenitor cluster, creating tangentially longer epicyclic loops. Stars released with energies further in excess of the critical escape energy of the cluster will perform epicycles with higher radial amplitudes. When comparing the two time snapshots of the in the N-body simulation in Figure 5.2, we see that because the cluster's

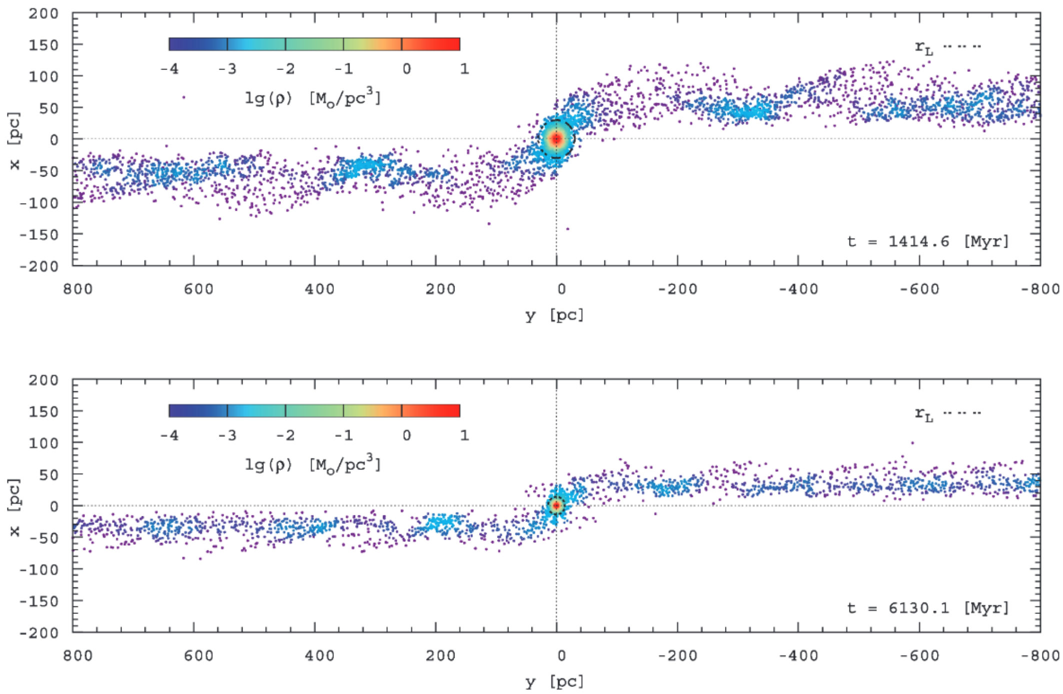

Figure 5.3: From Just et al. (2009), epicycle structure of an N-body stream at an early time with 50% of the initial mass still bound (top) and at a late time with only 10% of the initial mass still bound. The points are color-coded by the local density.

tidal radius has decreased at late times due to its mass loss, the radial offset of stars escaping the cluster has also decreased, shortening the tangential length of the epicycles as expected. The radial amplitude of the epicycles is smaller at late times as well, due to a dwindling number of stars in the cluster with energies far in excess of that required to escape.

Author's note: This description of the manifestation of epicycles in streams has remained largely qualitative, because actually deriving analytic descriptions of the paths of stars executing epicycles in streams relative to a progenitor cluster involves coordinate transformations that I personally find very confusing. The earliest derivation of an epicyclic stream path in a reference frame corotating with the progenitor cluster that I can find is in Küpper et al. (2008), where the cluster and host potentials are treated as point masses. Just et al. (2009) offer a much more comprehensive analytical treatment that is not limited to point mass potentials, and Amorisco (2015) sort of describe epicycles in streams in terms of action-angle formalism. The point is that it is possible, but for now, parsing the details is left as an exercise to the reader :)

5.3 Eccentric Orbits and the Formation of Feathers

5.3.1 Streaklines

Hot off the successes of several epicycle papers, Küpper and friends set out to explain the dynamics of substructure in streams on eccentric orbits in Küpper et al. (2012). In this case there are no analytical equations of motion for escaping stars, and instead they implement a "streakline" technique. As the cluster's orbit is integrated in an axisymmetric potential, test particles are generated and released with zero velocity offset to the cluster orbit and at its tidal radii. Then, at some late time, we can display the positions of all of the released stars relative to the potential as an infinitely cold approximation to the stream path. This was the predecessor to today's "particle spray" mock streams, where instead test particles are generated with some distribution of rates and release conditions calibrated to match stream morphologies from N-body simulations.

After successfully reproducing the predicted shapes of epicycles on a circular cluster orbit with streaklines, Küpper et al. (2012) move onto an eccentric cluster orbit. Shown in Figure 5.4 is the resulting streakline stream overlayed on an N-body model with the same cluster orbit at four different orbital phases. Despite not being in the nearly-circular orbit regime, we see that the streaky features and density variations in the N-body data are well-described by loops in the streaklines. At apocenter, the loops have the appearance of feathers, or elongated epicycles, and at all other orbital phases, the loops are collapsed down and folded over eachother so that they manifest as over- and underdensities of stars along the stream. Küpper et al. (2012) conclude that all feathering structure, as well as over- and underdensities along streams of all orbits can be attributed to epicyclic motion.

5.3.2 Aside on stream formation in action-angle space

Here it unfortunately becomes relevant to revisit the concept of action-angle formalism, as it relates to stream formation. Eyre & Binney (2011) provide a relatively useful summary, which Fardal et al. (2015) summarize and expand upon.

Recall that actions $\boldsymbol{J}$ are constants of motion along an orbit and angles $\boldsymbol{\theta}$ are their conjugate coordinates, which evolve linearly in time:

$$\boldsymbol{\theta}(t) = \boldsymbol{\theta}(0) + \boldsymbol{\Omega} t. \tag{5.13}$$

Here $\boldsymbol{\Omega}$ is the time derivative of the angles, called the "frequency vector," and is related to

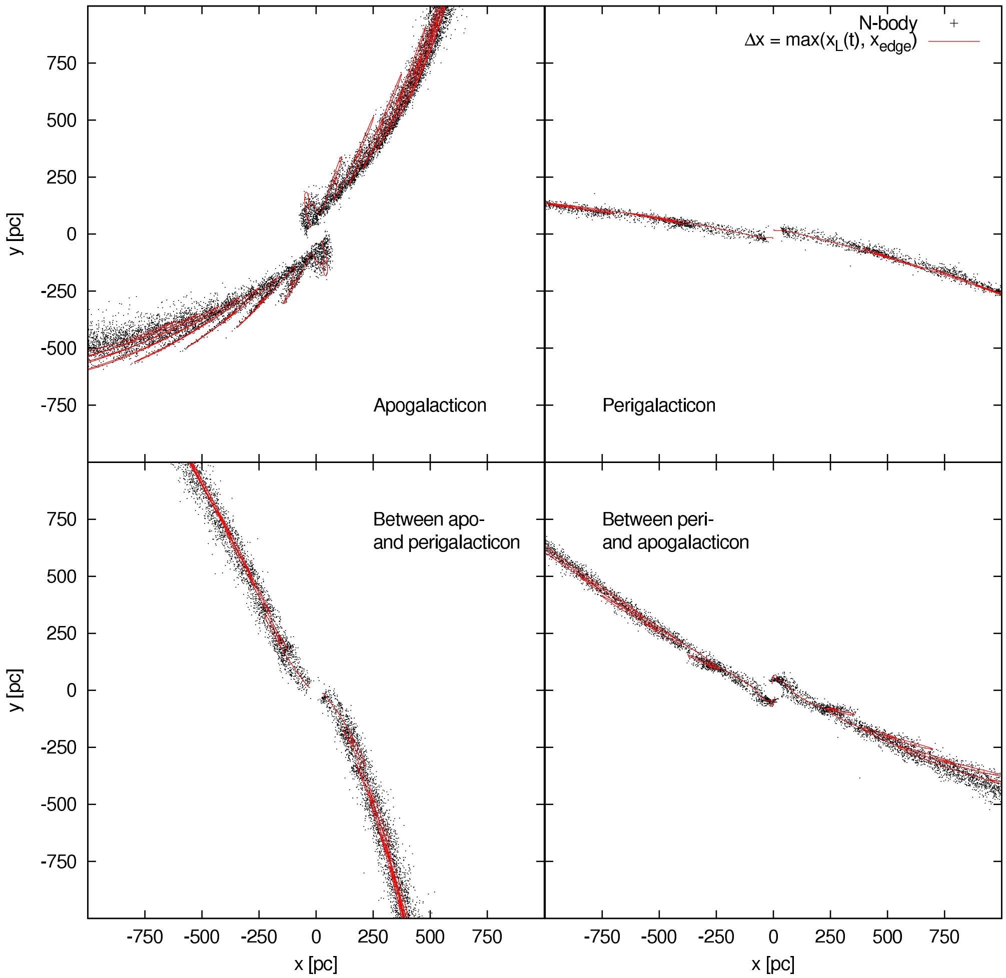

Figure 5.4: From Küpper et al. (2012), comparison of streakline results to N-body data for a cluster on an orbit of $e = 0.5$.

the actions by

$$\Omega_i(t) \equiv \dot{\theta} = \frac{\partial H}{\partial J_i}, \tag{5.14}$$

for Hamiltonian H. The derivative of the Hamiltonian with respect to the actions gives us the rate of change in the angles.

Now consider a star in a stream which no longer feels the effects of the cluster potential and orbits only in the host potential with Hamiltonian $H(\boldsymbol{J})$. The cluster itself is on an orbit with actions $\boldsymbol{J}_0$, and for actions near $\boldsymbol{J}_0$, the Hamiltonian can be approximated by a Taylor expansion:

$$H(\boldsymbol{J}) = H_0 + \boldsymbol{\Omega}_0 \cdot \delta \boldsymbol{J} + \frac{1}{2} \delta \boldsymbol{J}^T \mathbf{D} \delta \boldsymbol{J} \tag{5.15}$$

where $\delta \boldsymbol{J} = \boldsymbol{J} - \boldsymbol{J}_0$, $\mathbf{D}$ is the Hessian of H

$$D_{ij} = \left. \frac{\partial^2 H}{\partial J_i \partial J_j} \right|_{\boldsymbol{J}_0} \tag{5.16}$$

(analogous to a second derivative), and $\boldsymbol{\Omega}_0$ is the frequency vector of the cluster's orbit (Eq. 5.14 evaluated at $\boldsymbol{J}_0$).

So, the frequency vector $\boldsymbol{\Omega}$ of an orbit with action $\boldsymbol{J}$ is

$$\boldsymbol{\Omega}(\boldsymbol{J}) = \boldsymbol{\Omega}_0 + \mathbf{D}\delta\boldsymbol{J} \tag{5.17}$$

by Equation 5.14. For some spread in actions $\Delta\boldsymbol{J}$ and angles $\Delta\boldsymbol{\theta}_0$ relative to the progenitor cluster (corresponding to a spread in position and velocity of stream stars), the spread in angle space after some time t is given by

$$\Delta\boldsymbol{\theta}(t) = t\Delta\boldsymbol{\Omega} + \Delta\boldsymbol{\theta}_0, \tag{5.18}$$

where the spread in frequencies $\Delta\boldsymbol{\Omega}$ is related to the spread in actions by

$$\Delta\boldsymbol{\Omega} = \mathbf{D}\Delta\boldsymbol{J}. \tag{5.19}$$

When the spread in actions is large or the initial spread in angles is small (as is typical at cluster escape through the Lagrange points), the first term of Equation 5.18 dominates.

We see that a large spread in actions gives rise to a large spread in angles. Equivalently, an escaping star with large action offset from the progenitor cluster orbit will experience faster differential streaming and end up further away from the progenitor in angle space. Because energy and (at least one component of) angular momentum are themselves actions in axisymmetric potentials, I think it is equivalent (and definitely more intuitive) to frame this explicitly as the fact that stars escaping the cluster with higher energy or angular momentum offsets stream away from it faster and end up further along the tails of the stream.

Nonetheless, many dynamicists maintain that action-angle variables provide a superior description of stream structure. When modeling streams, Equation 5.13 allows us to compute particle positions as a simple linear function of time given the frequency vector and initial angle (as opposed to integrating the equations of motion in 3D), and to generate realistic mock streams, we need only to find realistic distributions of initial angle, frequency/action offset, and release time. In addition, Figure 5.5 is taken from Palau et al. (2025), who are attempting to illustrate the utility of action angle space in revealing the internal structure of as stream on an eccentric orbit. The left hand panels show the mass loss history of a globular

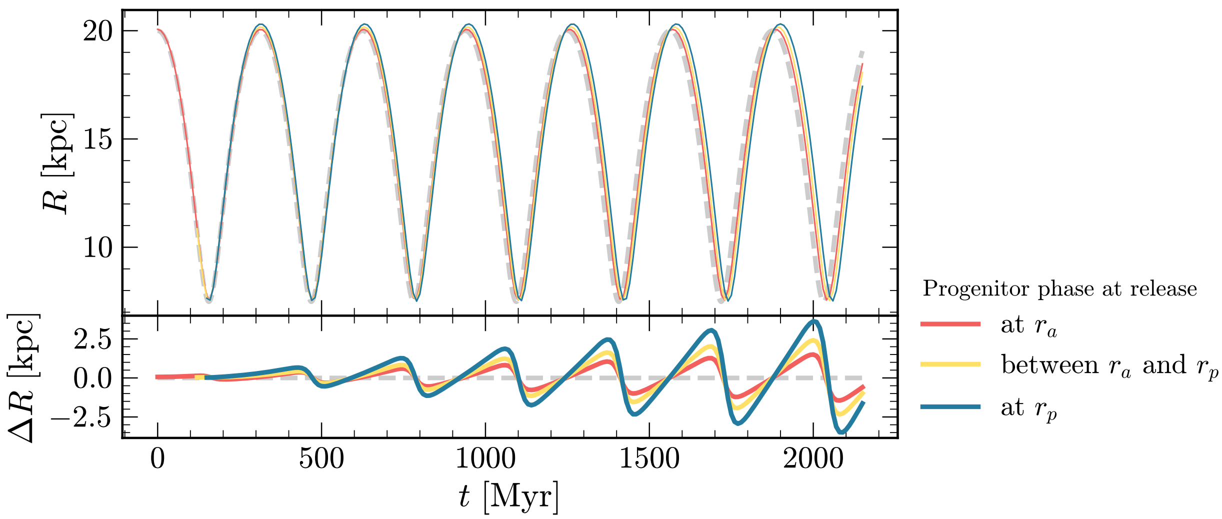

Figure 5.7: Three streakline particle trajectories from a cluster on an eccentric orbit in the disk: one particle released at apocenter, one at pericenter, and one at an intermediate time between the two.

the other hand, in the eccentric orbit/feathering case, overdense knots of stars are formed by escapers at the progenitor's apocenter, emitted with a smaller action offset, and lagging behind the ends of the feathers consisting of stars emitted at pericenter, which differentially stream away from the progenitor faster. The "same overdensities" in this case contain the same stars at all times, even as new feathers are added with each radial oscillation of the orbit. This is in contrast to the epicycles case, where all stars travel through both overdense and underdense regions.

In addition to the differential streaming, stars released from clusters on eccentric orbits do oscillate radially relative to the progenitor orbit, with oscillation amplitudes that depend on the release phase. Figure 5.7 is a half-baked attempt to demonstrate this, showing the radial positions of individual streakline particles over time generated for a cluster on an orbit in the disk of `MWPotential2014`, with $r_a = 20$ kpc, and $e \simeq 0.46$. Note that the apparent amplitude of the oscillations increases over time due to the fact that the radial periods of the released stars and the progenitor cluster become more and more out of phase.

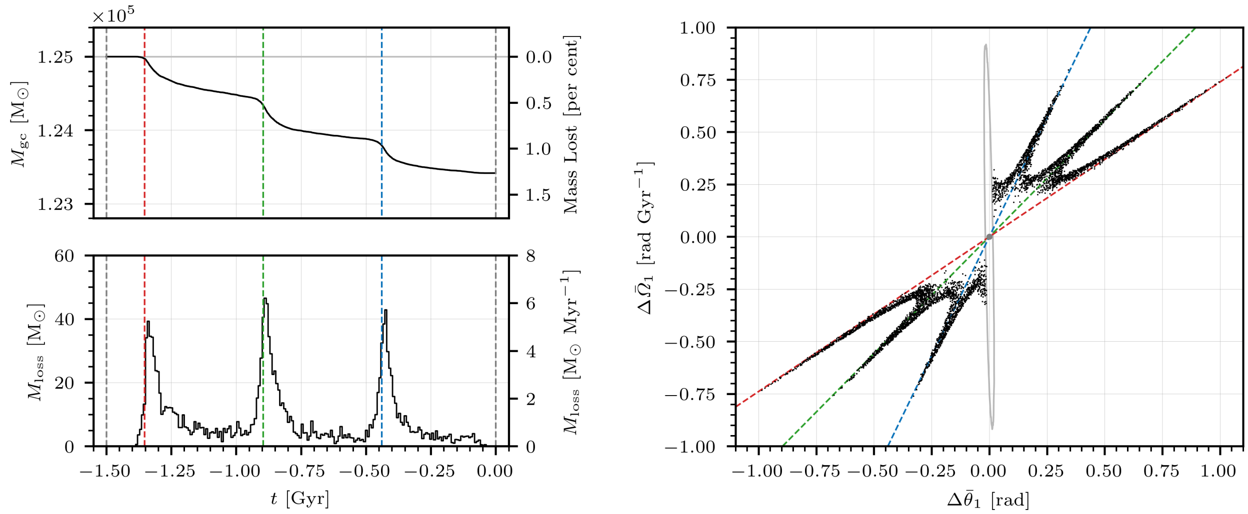

Figure 5.5: From Palau et al. (2025), Mass loss evolution (left) and escaped stars in angle-frequency space (right) of a simulated cluster on an eccentric orbit.

cluster on an eccentric orbit (with enhanced mass loss at each pericenter passage of the cluster due to tidal shocks). The right hand panel shows the stream stars in "angle-frequency" space, where the coordinates have been rotated to align with the stream's principle axis, and the subscript 1 denotes the component in the direction along the stream. We saw above that the frequency vector is related to the orbit actions, as stars with greater action offsets stream away from the cluster more quickly. The y-axis of Figure 5.5, the frequency, is the rate at which stars stream away from the progenitor cluster (related to the action offset), and the x-axis can be thought of as the distance along the stream. The dashed lines show the frequency offsets for stars released at successive pericenters distributed uniformly as a function of angle. We will see below that the spikey structures in this panel correspond to the "feather" structures seen in physical space, but that they are more obviously separated in angle-frequency space, and are not obscured by projection effects due to viewing angle.

5.3.3 Re-examining feathers and epicycles

On circular orbits, the action offsets from the progenitor cluster were very similar for each escaped star, meaning that each star entered the tails and streamed away from the progenitor at the same rate, and the position of a particle along a stream corresponded only to the escape time. For clusters on eccentric orbits, the changing strength of the potential leads to varied action offsets of escaping stars (in particular, varied energy and angular momentum offsets) depending on the orbital phase of the cluster at their time of escape. The consequence is that stars that escape at the cluster's pericenter stream away from the cluster faster than stars that escape at apocenter, forming the elongated feather structures attributed purely to epicyclic motion in Küpper et al. (2012).

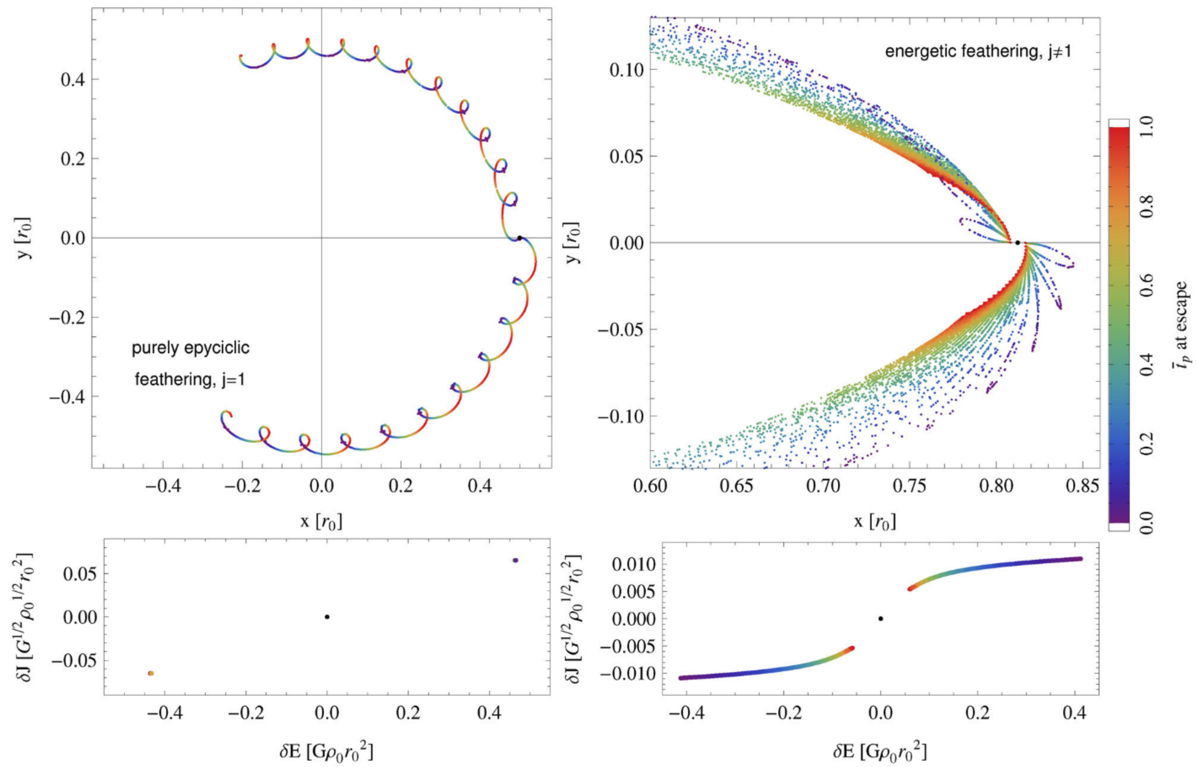

Figure 5.6: From Amorisco (2015), two streaklines illustrating the generation of purely epicyclic shapes in the case of a circular orbit (left), and of energetic feathers in the case of an eccentric orbit (right).

The distinction between feathering and pure epicyclic motion is examined in detail by Amorisco (2015). Shown in Figure 5.6, Amorisco (2015) have generated streaklines over the same amount of time for a circular orbit (left panels) and an eccentric orbit (right panels). The two orbits are chosen to share an azimuthal period, and the color of the streakline particles corresponds to the orbital phase of the right cluster (on the eccentric orbit) at the time of release ($\bar{t}_p = 0$ for pericenter, and $= 1$ for apocenter). The lower panels show the angular momentum and energy offsets from the progenitor orbit of the released particles, where we can see that in the circular case all particles have been released with the same offsets, and in the eccentric case, the offset follows a direct correspondence with the progenitor orbital phase at escape.

In the circular orbit/epicycle case, each cusp/overdensity of stars is located at a fixed location with respect to the progenitor. Because stream members systematically move away from the progenitor at the same rate, the cusp locations contain different stars at different times. On

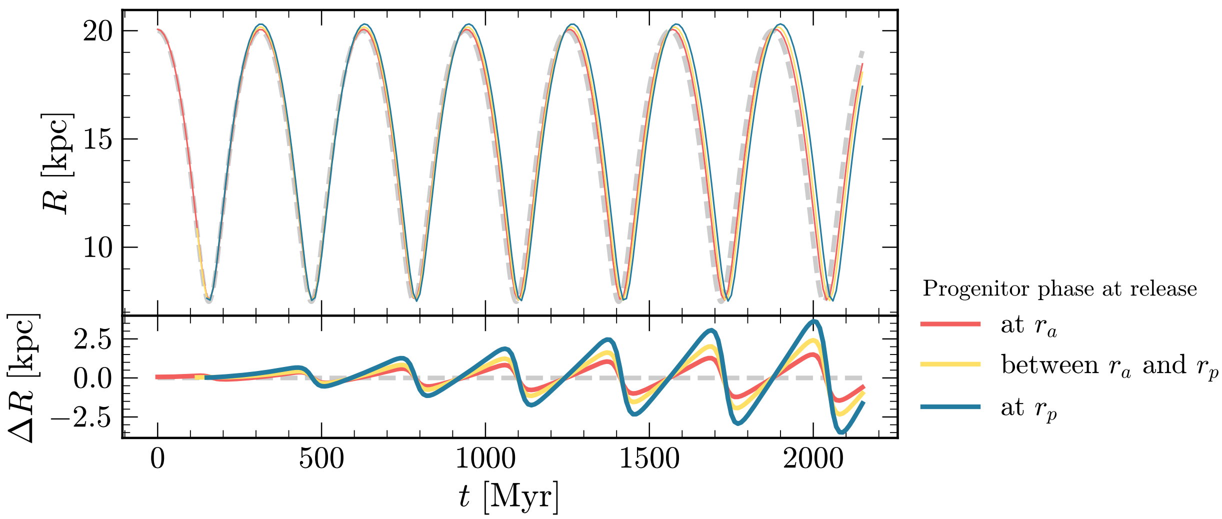

Figure 5.7: Three streakline particle trajectories from a cluster on an eccentric orbit in the disk: one particle released at apocenter, one at pericenter, and one at an intermediate time between the two.

the other hand, in the eccentric orbit/feathering case, overdense knots of stars are formed by escapers at the progenitor's apocenter, emitted with a smaller action offset, and lagging behind the ends of the feathers consisting of stars emitted at pericenter, which differentially stream away from the progenitor faster. The "same overdensities" in this case contain the same stars at all times, even as new feathers are added with each radial oscillation of the orbit. This is in contrast to the epicycles case, where all stars travel through both overdense and underdense regions.

In addition to the differential streaming, stars released from clusters on eccentric orbits do oscillate radially relative to the progenitor orbit, with oscillation amplitudes that depend on the release phase. Figure 5.7 is a half-baked attempt to demonstrate this, showing the radial positions of individual streakline particles over time generated for a cluster on an orbit in the disk of `MWPotential2014`, with $r_a = 20$ kpc, and $e \simeq 0.46$. Note that the apparent amplitude of the oscillations increases over time due to the fact that the radial periods of the released stars and the progenitor cluster become more and more out of phase.